Thin Film Morphologies of Block Copolymers Complexed with Wedge-Shaped Liquid Crystalline Amphiphilic Molecules

Krystyna Albrecht,[†] Ahmed Mourran,[†] Xiaomin Zhu,[†] Tommi Markkula,[‡] Juergen Groll,[†] Uwe Beginn,[†,§] Wim H. de Jeu,[‡] and Martin Moeller*,[†]

DWI an der RWTH Aachen e.V. and Institute of Technical and Macromolecular Chemistry at RWTH Aachen, Pauwelsstr. 8, D-52056 Aachen, Germany, and FOM-Institute for Atomic and Molecular Physics (AMOLF), Kruislaan 407, 1098 SJ Amsterdam, The Netherlands

Received June 14, 2007; Revised Manuscript Received January 8, 2008

ABSTRACT: Wedge-shaped molecules with a sulfonic group at the tip have been incorporated into a poly(2-vinylpyridine)-*b*-poly(ethylene oxide) (P2VP-*b*-PEO) diblock copolymer via proton transfer at different degrees of neutralization. The protonation of P2VP was monitored by means of Fourier transform infrared spectroscopy and X-ray photoelectron spectroscopy. The thin film morphology of the complexed block copolymers has been studied by scanning force microscopy and X-ray reflectivity. The complexes exhibit strongly microphase-segregated patterns comprising smectic layers of the complexed P2VP blocks, oriented parallel to the substrate throughout the whole film with the embedded PEO domains. For the complex with a degree of neutralization of 0.50 ordered amorphous PEO cylinders are observed oriented perpendicular to the substrate. For a degree of neutralization equal to 0.25 initially also perpendicular PEO cylinders are formed, but upon solvent-vapor annealing they partially merge, resulting in a mixed lamellar−cylindrical morphology. In all cases an extra surface layer is formed at the substrate. Thus, for the first time we have demonstrated that a block copolymer thin film structure can easily be controlled by the degree of neutralization of one of the blocks.

Introduction

The covalent connection of two chemically different and incompatible polymer chains compels linear diblock copolymers (BC) to self-assemble into ordered nanostructures. Depending on the volume ratio of the blocks and the Flory−Huggins interaction parameter χ, body-centered cubic, hexagonal-packed cylinders, and bicontinuous and lamellar morphologies have been predicted by theory and observed experimentally. The ordered microdomain structures span a range from 10 up to 100 nm, which makes these materials attractive for the design of materials with nanometer scale accuracy.[1,2] The majority of BC applications described in literature rely on controlled structure formation at surfaces.[3] In thin films, however, the behavior of BC differs from that in the bulk since the domain structure depends both on the surface energies and on the geometrical constraints. For lamellar structures, in films with a thickness in the range of one up to a few multiples of the bulk periods preferential segregation of one of the blocks to the substrate and/or the air interface will favor parallel orientation of the microdomains. As a result, the film thickness adjusts to a set of discrete values of the bulk period and incomplete top layers yield a surface topography with islands or holes with a height equal to this period.[4]

While phase segregation occurs spontaneously and mesophase ordering of the microdomains can be controlled rather well for solution-cast thin films, to obtain a uniform orientation of the microdomains normal to the film surface—as required in certain applications—remains a challenge. Some success has been achieved by the introduction of external stimuli during the processing steps such as mechanical forces[5] or electrical fields,[6,7] adjusting surface interactions[8−10] and film thickness,[11,12] as well as by fast solvent evaporation.[13−15]

Incorporation of side-chain liquid crystalline fragments into BC leads to greater structural complexity and functionality since microdomain ordering is affected by competition between two inherently different length scales. Smectic liquid crystalline (LC) side-chain homopolymers self-organize on length scales from 0.5 to 5 nm corresponding to the inter-mesogen distance and the smectic layer periodicity, respectively. Thus, for LC side chain BC (LC−BC) two different ordering mechanisms occur within a single system, with length scales in the range of 0.5−100 nm.[16−18] For such LC−BC the LC field can affect mesophase formation and domain orientation, and in thin films thermally stable morphologies can be generated consisting of lamellae and cylinders oriented perpendicular to the surface.[19−23]

In all above-mentioned examples the hierarchical order is due to covalently bonded mesogenic side groups. An elegant alternative for obtaining hierarchically structured materials based on BC and oligomeric amphiphiles has been successfully applied by Ikkala et al.[24] In their work self-organization on two length scales is obtained by incorporation sterically demanding moieties to BC via hydrogen bonding, ionic, and coordination interactions. Only a few papers have been published so far on the thin film structures by such types of system. Thin films of cylinder-forming supramolecular assemblies of hydrogen-bonded poly(styrene)-*block*-poly(4-vinylpyridine) copolymers with 2-(4′-hydroxybenzeneazo)benzoic acid were investigated by Stamm et al.[25] The orientation of the cylinders depended on the solvent used for casting and annealing. However, within the given morphology no hierarchical structures were observed.

Recently, we have developed a new class of wedge-shaped amphiphilic sulfonic acid molecules, which are able to self-assemble into lamellar or columnar liquid-crystalline structures and form supramolecular complexes with poly(4-vinylpyridine) (P4VP).[26,27] In the present work, the synthesis of a wedge-shaped amphiphilic sulfonic acid molecule with three octyl substituents

* Corresponding author. E-mail: moeller@dwi.rwth-aachen.de.
[†] RWTH Aachen.
[‡] AMOLF.
[§] Present address: Universität Osnabrück, Institut für Chemie, OMC, Barbarastr. 7, D-49076 Osnabrück, Germany.

10.1021/ma071317n CCC: $40.75
Published on Web 02/16/2008

Scheme 1. General Synthesis Strategy for the Preparation of the Complexes

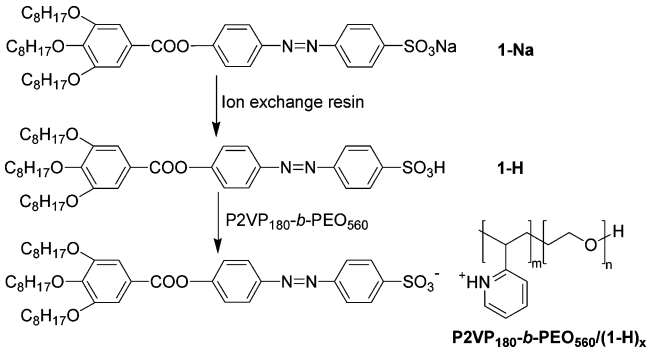

is described, which is linked to poly(2-vinylpyrydine)-*block*-poly(ethylene oxide) (P2VP-*b*-PEO) copolymer via an acid base interaction. Three complexes with different degrees of neutralization of the P2VP block have been prepared and analyzed by Fourier transform infrared (FT-IR) and X-ray photoelectron spectroscopy (XPS). X-ray reflectivity (XR) of supported thin films indicates that the complexes form smectic mesophase. The microphase separation in these films before and after vapor annealing has been studied by scanning force microscopy (SFM) techniques. As anticipated, variation in the degree of neutralization of P2VP and the associated change of the volume fraction of the blocks had a considerable influence on the morphology.

Experimental Section

Materials. Poly(2-vinylpyridine)-*block*-poly(ethylene oxide) copolymer with a monomer ratio 180/560, $P2VP_{180}$-*b*-PEO_{560}, and $M_w/M_n = 1.06$ was synthesized by sequential anionic polymerization similar to the procedure described before in tetrahydrofuran using diphenylmethylpotassium as an initiator.[28] Sodium {4′-[3″,4″,5″-tris(octyl)benzoyloxy]azobenzene-4-sulfonate} **(1-Na)** was synthesized according to the procedure described elsewhere.[26] Silicon wafers (100) were purchased from CrysTec GmbH. Syringe filters (0.2 μm, PTFE) were obtained from Wheaton. Acetone, isopropanol, ethanol, chloroform, diisopropyl ether, benzene (Merck, p.a.), and ion-exchange resin (Amberlyst 15, Aldrich) were used as received.

Polymer Complex Preparation. The synthesis of polymer−sulfonic acid complexes is outlined in Scheme 1. A solution of sodium sulfonate (**1-Na**) (100 mg) in diisopropyl ether (10 mL) was shaken over night with ion-exchange resin (1 g). Subsequently, the resulting solution was filtered through a glass filter (pore size 4), and the ion-exchange resin was washed three times with diisopropyl ether (5 mL). The combined filtrates were added to a well-stirred solution of P2VP-*b*-PEO (30.7 mg for complex $x = 1$; 61.4 mg for complex $x = 0.5$, 122.8 mg for complex $x = 0.25$) in chloroform (concentration of the copolymer was always 0.5 mg/mL). The resulting solution was stirred for an additional 2 h. Then the solvent was removed under reduced pressure using a rotor evaporator. The products were dried in vacuum at 40 °C. Yield: 93−97%.

Film Preparation. Silicon wafers were cut into pieces of 10 × 15 mm^2 with a diamond knife and cleaned by sonication in acetone, water, and isopropanol for 2 min each, followed by drying in a stream of nitrogen. Stock 20 g/L solutions of the pure $P2VP_{180}$-*b*-PEO_{560} copolymer and $P2VP_{180}$-*b*-$PEO_{560}/(1\text{-H})_x$ complexes were prepared in chloroform. Prior to dipping of the substrates the solutions were filtered through 0.2 μm PTFE syringe filters. Films were obtained by dipping cleaned substrates into the polymer solution with an immersion and withdrawal speed of 45 mm/min. The effect of the polarity of the surface has been carefully examined by UV/ozone treatment for 12 min of the silicon oxide surface. Regardless the cleaning procedure, the contact angle with water was below the detection limit in both cases, and we did not observe any effect of the substrate treatment on the surface morphology.

For equilibration the samples were exposed to saturated benzene vapor in a closed vessel at room temperature. The duration of the exposure was varied. After solvent vapor exposure, the samples were removed to ambient atmosphere and carefully dried with nitrogen.

Ellipsometry. Layer thicknesses were determined using a MM-SPEL-VIS ellipsometer from OMT. The silicon substrates were examined with a spectral method in the wavelength range from 450 to 900 nm. The azimuthal angle was kept at 15°. The integration time was dependent on the layer thickness and the resulting signal intensity. The main source for systematic errors during the measurements is the correct position of the sample. This results in uncertainties in both the angle of incidence and the azimuthal angle. This error has been minimized by measuring all samples within one session right after another with exactly the same geometry of the device and positioning of the sample holder. Each single measurement averaged over the area of 3 × 5 mm^2. In addition, to further reduce systematic errors in the data collection, always a clean substrate was measured as reference for a series of experiments. Statistic errors are thus small and have been evaluated by measuring on each sample five different areas. The data as presented are average values of each sample while statistical errors for all samples are <1 nm.

Fourier Transform Infrared Spectroscopy (FT-IR). FT-IR spectra were recorded on a Nicolet 710 FT-IR spectrometer by means of photoacoustic techniques. A few milligrams of dried samples was put in small aluminum pans and then used for the examination.

X-ray Photoelectron Spectroscopy (XPS). XPS measurements were carried out in an Ultra AxisTM spectrometer (Kratos Analytical, Manchester, UK). The samples were irradiated with monoenergetic Al K*1,2 radiation (1486.6 eV), and the spectra were taken at a power of 144 W (12 kV × 12 mA). The aliphatic carbon (C−C, C−H) at a binding energy of 285 eV (C 1s photoline) was used to determine the charging. The spectral resolution, i.e., the full width of half-maximum (fwhm) of the ester carbon from PET, was better than 0.68 eV for the elemental spectra. The emission angle of electrons was set at 90° with respect to the sample plane, which results in an information depth of about 10 nm for polymer samples.

Scanning Force Microscopy (SFM). SFM studies were conducted using a Nanoscope IIIa from Digital Instruments operating in the tapping mode. Standard silicon cantilevers were used (PPP-NCH from Nanosensors) with a spring constant $k \approx 42$ N/m and an oscillation frequency $f_0 \approx 330$ kHz. Height and phase images were recorded simultaneously at a scan rate of 1 Hz. All measurements were performed at amplitude A_0 of the freely oscillating cantilever of 30−50 nm. Set-point amplitudes A_{sp} were in the range of $0.85-0.95A_0$ and $0.35-0.45A_0$, corresponding to *light-tapping* and *hard-tapping* conditions, respectively.[29] The in-plane average center-to-center distance L was determined from the position of the maximum of the power spectral density (PSD) of a 2 × 2 μm^2 height and phase image. The PSD was calculated using the Nanoscope software (version 5.12r3). The uncertainty in the lateral dimensions was estimated as a half-width of the peak in PSD.

X-ray Reflectivity (XR). XR was performed using an in-house setup at the FOM Institute AMOLF at a rotating anode X-ray generator (Rigaku RU-H300) operating at 18 kW. By employing a W/B_4C graded parabolic multilayer mirror (Osmic, Auburn Hills) the Cu Kα radiation was collimated in the scattering plane (*xz*-plane, with the *z*-axis along the film normal). The samples were mounted vertically at the center of a two-circle goniometer and investigated under specular reflection conditions. Additional pre-sample and predetector slits resulted in an overall resolution in the horizontal scattering plane of $\Delta q_z = 0.03$ nm^{-1}. The intensity was integrated over the broad resolution in the vertical *y*-direction. In reciprocal space specular reflectivity scans probe the scattered intensity along q_z. The X-ray intensity was corrected for sample size effects at small incidence angles as well as for background scattering. The data were analyzed using an iterative matrix formalism derived from the Fresnel equations. The calculated

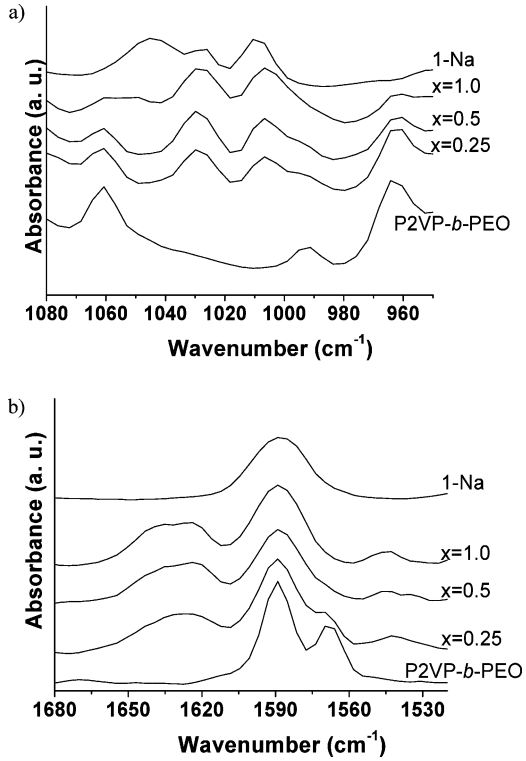

Figure 1. Infrared spectra of $P2VP_{180}$-*b*-PEO_{560}/(1-H)$_x$, $P2VP_{180}$-*b*-PEO_{560}, and 1-Na (a) for the 950−1080 cm^{-1} region and (b) for the 1520−1680 cm^{-1} region.

reflectivity profiles were convoluted with the experimental resolution, assumed to be of Gaussian statistics.

Results and Discussion

Characterization of the Complexes. One of the basic tasks is to assess the degree of neutralization of the pyridine groups by the sulfonic acids. FT-IR spectroscopy combined with XPS allows sensing the chemical structure of given species in bulk and in thin layers, respectively. The complexes of $P2VP_{180}$-*b*-PEO_{560} with 25%, 50%, and 100% neutralized vinylpyridine units will be denoted as $P2VP_{180}$-*b*-PEO_{560}/(1-H)$_{0.25}$, $P2VP_{180}$-*b*-PEO_{560}/(1-H)$_{0.5}$, and $P2VP_{180}$-*b*-PEO_{560}/(1-H)$_1$, respectively.

FT-IR is a suitable tool to analyze the proton-transfer process. Because of the chemical instability of the sulfonic acid **(1-H)** in the dried state,[26] its sodium salt **(1-Na)** has been used as reference. Earlier infrared studies showed that in the case of P2VP the stretching modes of the pyridine ring at 1570, 993, and 625 cm^{-1} are shifted toward higher frequencies upon hydrogen bonding with poly(ethylene-*co*-methacrylic acid).[30] The same bands are also affected upon proton transfer in the complexes studied here. Figure 1 shows the spectra of the $P2VP_{180}$-*b*-PEO_{560}/(1-H)$_x$ complexes ($x = 0.25$, 0.5, and 1) and for comparison the spectrum of pure $P2VP_{180}$-*b*-PEO_{560} copolymer and **1-Na**. Figure 1a indicates that the band observed at 993 cm^{-1} for the pure polymer gradually weakens with increasing degree of neutralization and disappears at 100% (complex $P2VP_{180}$-*b*-PEO_{560}/(1-H)$_1$). As also depicted here, Ikkala et al. observed that upon proton transfer this band is replaced by two bands with similar strengths at 1008 and 1033 cm^{-1}.[31] Figure 1b presents detailed spectra recorded at 1520−1680 cm^{-1} showing that the band observed for the pure polymer at 1570 cm^{-1} has been replaced by a band at 1635 cm^{-1} for the protonated complexes. This new band appearing at 1635 cm^{-1} is quite broad and obviously splits into two distinct bands as the degree of neutralization is enhanced. Similar observation has been reported earlier.[31,32] So far, the IR spectra give a clear indication of complexation of the pyridine groups with the wedge-shaped ligand.

XPS has been successfully used to quantify different chemical interactions of the nitrogen atom in a pyridine ring.[33] Films of thickness between 25 and 47 nm (see Table 1) of pure $P2VP_{180}$-*b*-PEO_{560} as well as $P2VP_{180}$-*b*-PEO_{560}/(1-H)$_x$ complexes cast on cleaned silicon wafers were investigated in order to determine the degree of neutralization of P2VP. Figure 2 displays spectra for the relevant electron binding energy gap of 402−399 eV arranged according to increasing protonation ratio (degree of neutralization) (Figure 2a−d). To determine the peak position, the experimental curves were fit by a Gaussian function. The N 1s peak of unprotonated pyridine units of P2VP is observed at 398.9 eV. Upon P2VP neutralization with 1-H two additional peaks appear at 399.9 and 401.2 eV, which correspond to the N 1s in the azo and pyridinium groups, respectively. With increasing degree of neutralization the relative intensity of the N 1s peak at 398.9 eV gradually decreases, while the high-energy peaks corresponding to azo and the pyridinium groups increase. Table 1 summarizes the degrees of neutralization derived from the XPS spectra by integration of the areas under the N 1s peaks at 398.9 and 401.2 eV. The volume fractions of PEO (Φ_{PEO}) calculated from the XPS data are also presented in Table 1. The latter compare quite well with the values expected from the block lengths. The ratio of the peak intensity of pyridinium to the azo groups should be 1:2. This is clearly demonstrated at the degree of neutralization of 25% (Figure 2b). In the case of the sample with 100% protonated P2VP units (Figure 2d) the XPS spectra, however, indicate more sulfonic acid molecules than pyridinium units based on the measured intensity ratio of the XPS pick at 399.9−401.2 eV. Hence, it must be concluded that the pyridine groups are not fully neutralized, and the remaining pyridine signal at 398.9 eV is lost in the noise level.

Thin Films. In this section we investigate the self-assembly of the BC complexes with different degrees of neutralization in thin films by XR and SFM. Thin films of P2VP-*b*-PEO/(1-H)$_x$ were prepared by dipping silicon oxide substrates into solutions of the BC complexes with the concentration of 20 g/L. The film thickness of the original series 1 investigated by SFM was determined by ellipsometry (see Table 1). In addition the thickness of a second series 2 prepared later for XR studies are given. The results are very comparable, showing that the

Table 1. Degree of Neutralization of the P2VP with 1-H Determined from XPS Measurements at Given Film Thickness and the Corresponding PEO Volume Fractions and Molecular Mass

sample	film thickness (nm) series 1[a]	film thickness (nm) series 2[b]	degree of neutralization of P2VP units[c]	Φ_{PEO}[c]	M_n [g/mol]
$P2VP_{180}$-*b*-PEO_{560}	25	31	0	0.59	43 600
$P2VP_{180}$-*b*-PEO_{560}/(1-H)$_{0.25}$	47	48	0.22	0.34	72 900
$P2VP_{180}$-*b*-PEO_{560}/(1-H)$_{0.5}$	45	44	0.58	0.20	120 900
$P2VP_{180}$-*b*-PEO_{560}/(1-H)$_1$	43	41	<1	0.14	176 800

[a] Ellipsometry; used in the SFM studies, statistical error for all samples is <1 nm. [b] X-ray reflectivity. [c] Estimated from XPS data.

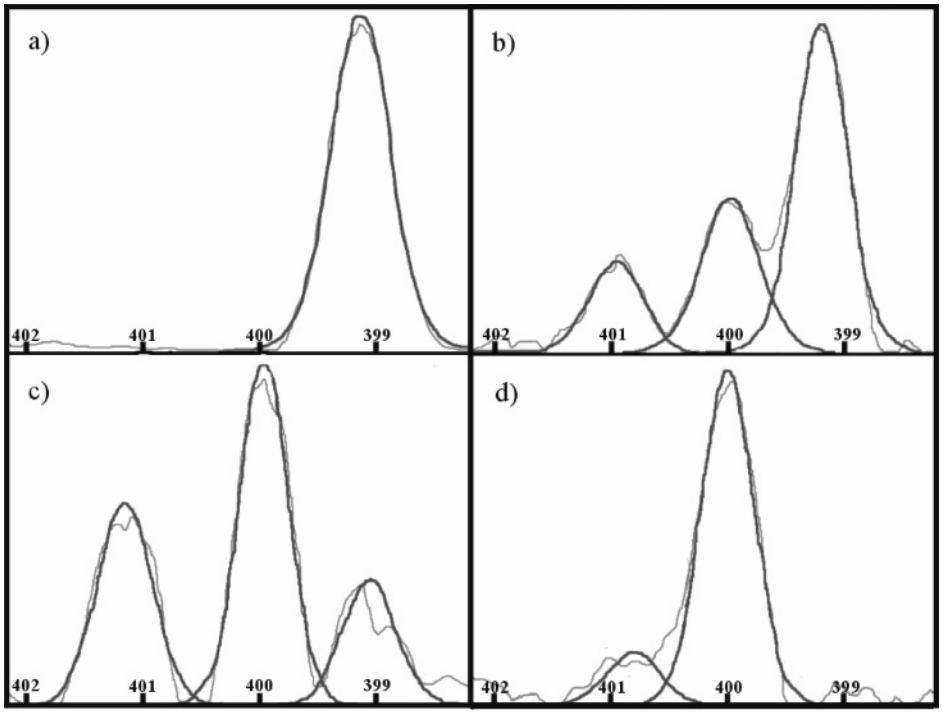

Figure 2. XPS data (brighter line) and Gaussian fits (darker line) of (a) $P2VP_{180}$-*b*-PEO_{560}, (b) $P2VP_{180}$-*b*-$PEO_{560}/(1\text{-H})_{0.25}$, (c) $P2VP_{180}$-*b*-$PEO_{560}/(1\text{-H})_{0.5}$, and (d) $P2VP_{180}$-*b*-$PEO_{560}/(1\text{-H})_1$. Units on the *x*-axis are in eV, the intensity of the signals is displayed in arbitrary units ($N_{pyridine}$ at 398.9 eV, N_{azo} at 399.9 eV, and $N_{pyridinium}$ at 401.2 eV).

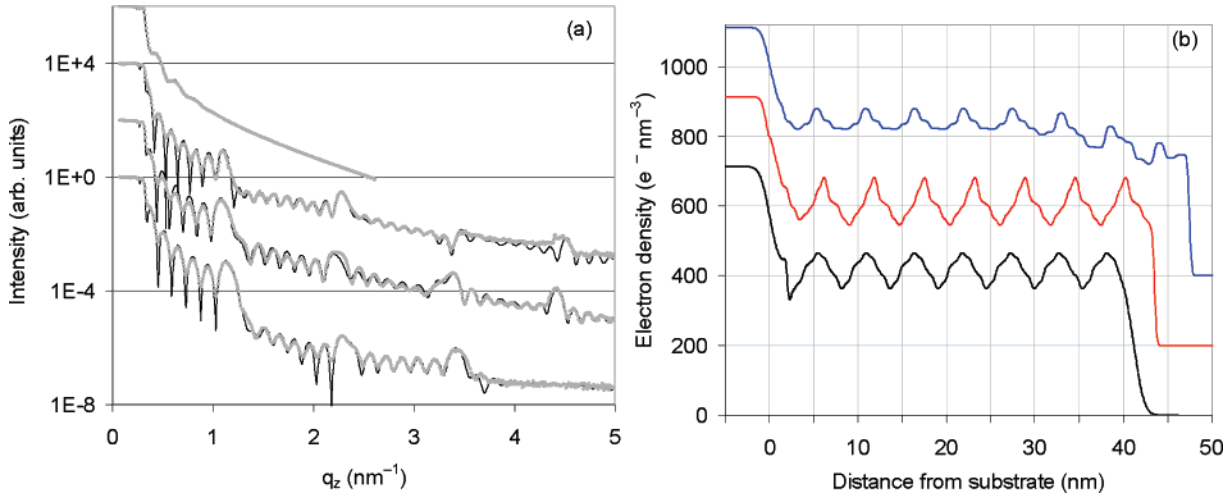

Figure 3. X-ray reflectivity data for films of $P2VP_{180}$-*b*-$PEO_{560}/(1\text{-H}))_x$. (a) Normalized intensity for $x = 0$, 0.25, 0.5, and 1.0 (from top to bottom). The curves are displaced vertically by 2 decades for clarity. Open circles represent experimental data and solid lines the fits. (b) Density profiles corresponding to the fits shown in (a); $x = 0.25$, 0.5, and 1.0 (from top to bottom). The curves are displaced by 135 e^-/nm^3 for clarity.

procedure of filmmaking is reproducible. Note that at a given solution concentration the films formed by the BC complexes have a similar thickness, while the pure $P2VP_{180}$-*b*-PEO_{560} yields thinner films. We speculate that the presence of low molecular weight ligands alters the viscosity or the shape of the meniscus bridging the bulk solution and the substrate, which may increase the deposited amount during the dip-coating process.

In general, BC morphologies in thin films become more perfect after vacuum annealing above any glass transition temperature. For films of the complexed P2VP-*b*-PEO/$(1\text{-H})_x$, however, extended annealing at 170 °C for 48 h did not significantly influence the morphology. Thus, in this work "equilibration" has been performed by exposing the samples to a saturated atmosphere of a nonselective solvent.[34] Benzene was chosen since it is a good solvent for both blocks of the copolymer as well as for the P2VP/1-H complex segments.

X-ray Reflectivity. Before investigating the films of series 2 by XR, they were also checked by SFM and found to exhibit similar morphologies as the original series 1 studied extensively by SFM (to be discussed hereafter). The XR data are presented in Figure 3 together with results from the fits. The thickness of the respective films as given in Table 1 is directly inferred from the period of the Kiessig fringes. Most importantly, for all degrees of neutralization Bragg-like peaks are seen, indicating unambiguously that 7−8 layers of period $d = 5.55 \pm 0.15$ nm are systematically parallel to the film interfaces. From the occurrence of several higher harmonics we conclude that the layers are very well organized. Furthermore, an additional surface layer is observed at the substrate with a thickness of 0.4−0.7 times the smectic period (see Table 2). Note that the information in Table 2 is independent of the model used for the fits leading to Figure 2b. For 25% complexing the substrate

Table 2. Layer Structure from X-ray Reflectivity

degree of complexing (%)	no. of layers	periodicity (nm)	bottom layer (nm)
25	8.48	5.52	2.63
50	7.66	5.68	3.77
100	7.43	5.44	2.35

layer thickness corresponds to $d/2$ within 5%. For 50% and 100% neutralization, the thickness of the substrate layers deviates from $d/2$. The smectic layer period d hardly varies in spite of a considerable change in the degree of neutralization from 25% to 100%. This is in contrast with our recent studies on P4VP complexes with 4′-[3″,4″,5″-tris(dodecyloxy)benzoyloxy]azobenzene-4-sulfonate and **1-H**, where we observed a slight but systematic decrease of the interlayer distances upon increasing the degree of neutralization.[27]

The data clearly indicate that the ordering of the ligands is a dominant effect controlling the morphology rather then any incompatibility between the polymer blocks. The layer periodicity $d = 5.55 \pm 0.15$ nm is close to twice the length of a **1-H** molecule with fully stretched alkyl chains, estimated to be 2.8 nm from space-filling models. Hence we conclude that the side groups in the complexes do not overlap and form close-packed layer structures.

Scanning Force Microscopy. Prior to the investigation of BC complexes, the film morphology of the pure $P2VP_{180}$-*b*-PEO_{560} was studied. Figure 4 presents SFM images of the $P2VP_{180}$-*b*-PEO_{560} copolymer obtained before and after vapor annealing. The freshly cast samples depicted in Figure 4a show that the BC crystallizes as expected from the relatively large volume fraction of PEO. The crystallization pattern indicates that the PEO chains form lamellae oriented normal to the substrate surface, so-called "edge-on" morphology. Upon vapor annealing the PEO chains reorient into the "flat-on" morphology with the lamellae oriented parallel to the surface. Above the melting point of PEO thin films of $P2VP_{180}$-*b*-PEO_{560} BC do not show any features associated with microphase separation; the same behavior was observed in thicker films up to 100 nm. These results are in agreement with XR showing that the blocks are likely to be miscible. The Flory−Huggins parameter of the BC is not known, and most reports in the literature deals with lower molecular weight that are indeed miscible.[35] This property of the thin BC films is in contrast to copolymers containing incompatible amorphous−crystalline blocks, wherein both microdomain formation and crystallization concur for ordering.[36]

Neutralization with wedge-shaped sulfonic acid molecules alters the polar P2VP block due to the hydrophobic alkyl tails. Hence, in combination with the smectic ordering of the wedge-shaped sulfonic acid parts considerable changes of the surface properties are expected. Figure 5 shows the SFM image of $P2VP_{180}$-*b*-PEO_{560}/$(1\text{-H})_{0.25}$ films recorded with *light tapping* during which the SFM probe exerts a minimum force onto the surface. In this case the phase image is nearly featureless, and the topography image reveals islands with a height of 5.9 ± 0.4 nm, originating from an incomplete smectic top layer. Similar results are obtained for the films of the $P2VP_{180}$-*b*-PEO_{560}/$(1\text{-H})_{0.50}$ complex. Note that the ligand is a wedge with three C8 aliphatic chains at its periphery. The alkyl chain with the lower surface energy in the system segregates to the air interface and form a surface layer. However, a slight increase (less than 10%) of the set point amplitude enhances the contrast, as illustrated in the micrographs of Figures 6 and 7. Both compositions 25% and 50% display two structural features: surface layering and an in-plane structure distinctive for microphase segregation. Improved ordering was achieved after vapor annealing, suggesting a release of the kinetically trapped conformational stress arising from the casting process. Further annealing does not influence the final structure.

Being the minority phase, PEO is assigned to the dark contrast in the phase image while it is observed below the surface level in the height image. The phase contrast indicates that the PEO domains are softer than the P2VP/$(1\text{-H})_x$ matrix.[37] In-situ thermal treatment confirms the amorphous nature of the PEO. The morphology and the phase contrast do not change when the sample is heated to 100 °C, well above the melting temperature of PEO. We conclude that in thin films (<100 nm) of the complexed material crystallization of the PEO blocks is suppressed.[38] In contrast to these results, thermal analysis (not included) shows that in the bulk the PEO crystallizes in the BC complex.

The volume fraction of PEO in the $P2VP_{180}$-*b*-PEO_{560}/$(1\text{-H})_{0.25}$ BC complex suggests formation of PEO cylinders in the smectic LC matrix. From the in-plane ordering we anticipate the block interfaces to be orthogonal to the smectic layers which from XR data are known to be parallel to the film interfaces. Hence, SFM studies reveal mixed morphologies lamellae and cylinders oriented orthogonal to the substrate and air interface. In particular, from Figure 6c the formation of lamellae can be anticipated by merging adjacent PEO cylinders. After long "equilibration" times the mixed morphology persists, but the height variation is strictly reduced to the thickness of one smectic layer. The in-plane average center-to-center distance L equals 43 ± 3 nm for the lamellae and 46 ± 3 nm for the cylinders with an average cylinder diameter $D = 28 \pm 2$ nm (see Table 3).

Enhancing the degree of neutralization in the $P2VP_{180}$-*b*-PEO_{560}/$(1\text{-H})_{0.5}$ BC complex leads to the formation of a purely cylindrical microdomain structure. Both the freshly cast and the vapor-treated film show orthogonal orientation of the cylinders with respect to the film interfaces. Interestingly, the in-plane average center-to-center distance of the cylindrical domains is very similar to the one for 25% complexing (see Table 3) while the average cylinder diameter is appreciably *smaller*. After 12 h vapor annealing the $P2VP_{180}$-*b*-PEO_{560}/$(1\text{-H})_{0.5}$ BC complex shows smectic layering but with a nonuniform film thickness. In particular, elevations and depressions appear with a depth of 70 nm, exceeding both the initial film thickness and the BC in-plane periodicity. This behavior is typical for a dewetting process.[39] The vertical orientation of the cylinders does not depend on the film thickness (as studied up to 100 nm). Within the holes that result from dewetting a featureless surface layer is observed, indicated by an arrow in Figure 7b. The thickness of this layer, as determined from the SFM measurement, is 3.2 ± 0.2 nm, larger than the length of the sulfonic 1-H ligand. XR indicates for 50% complexing a substrate layer of 3.8 nm that is also appreciably larger than half the smectic period found for 25% complexing.

Finally we come to the fully neutralized complex $P2VP_{180}$-*b*-PEO_{560}/$(1\text{-H})_1$. According to the volume fraction of PEO, one would expect this system to form spherical PEO domains. However, X-ray reflectivity again demonstrates smectic layering but now with a decreased thickness of the bottom layer ($<d/2$). SFM images of the P2VP-*b*-PEO /$(1\text{-H})_1$ films are presented in Figure 8. Vapor annealing does not influence the surface morphology of the completely neutralized complex, and only SFM images of the freshly prepared sample are presented. Similar to the complexes with lower degree of neutralization, and consistent with the X-ray data, terraces are present with a

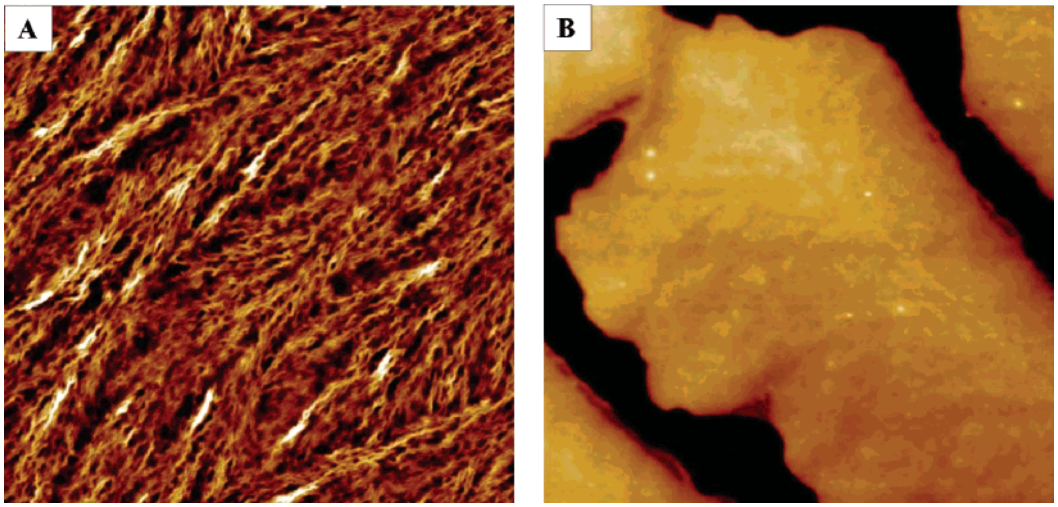

Figure 4. SFM height images of $P2VP_{180}$-*b*-PEO_{560} thin films (A) as prepared and (B) after benzene vapor annealing. *Z* range is 10 nm for (A) and 25 nm for (B) images. Scan size is $4 \times 4\ \mu m^2$.

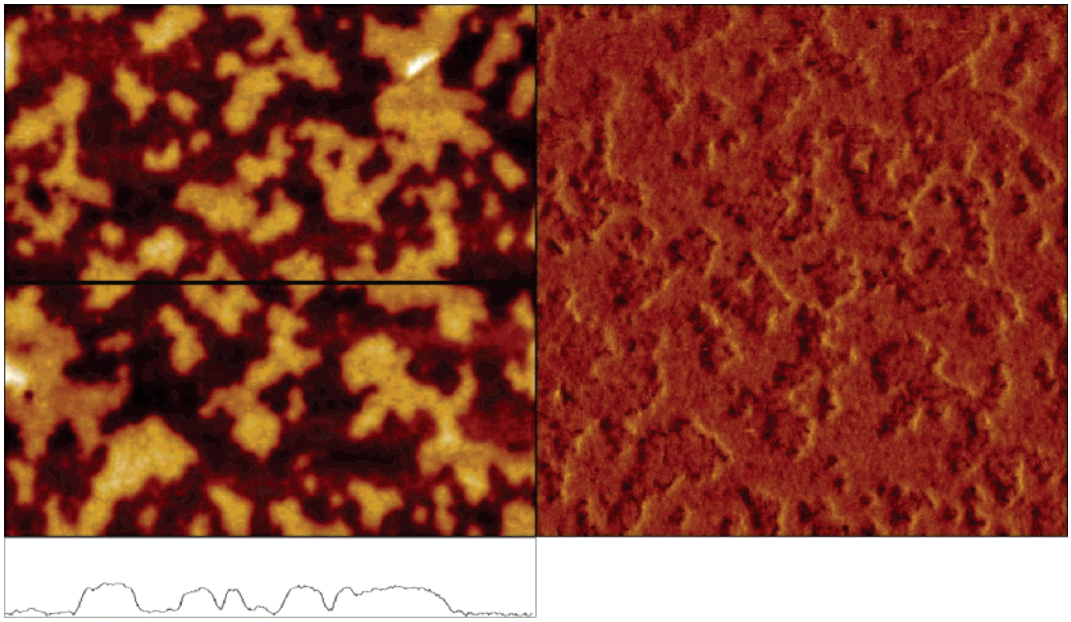

Figure 5. SFM images of $P2VP_{180}$-*b*-PEO_{560}/$(1\text{-H})_{0.25}$ complex recorded under *light tapping* conditions. *Z* range is 15 nm for height image (left) and 15° for phase (right). Scan size is $2 \times 2\ \mu m^2$.

height of 5.9 nm. However, the surface of the layers exhibits a second structural feature. The cross-section profile in Figure 8a demonstrates elevation or island at the surface of the terraces. This is illustrated by the height distribution depicted in Figure 8b, which shows two maxima separated by 2.2 and 3.6 nm. In addition, the phase image shows that the smooth areas between the islands are laterally structured with a periodicity of 12.2 nm (see Figure 8b PSD and the FFT in the inset). This in-plane repetition length of 12.2 nm is smaller than the block copolymer periodicity and larger than the smectic period.

Modeling. From X-ray reflectivity as well as from SFM, smectic layering is evident for all degrees of neutralization of the pyridine groups. Unambiguously, formation of PEO domains is observed for the two lower ratios. Scheme 2 gives two different models that can form a base for further discussion. The model assumes rather tight binding between the ligand (**1-H**) and the pyridine groups of the polymer backbone. This is relevant since the heat of interaction ligand−pyridine is of the order of 20 k_BT (k_BT denoting the thermal energy).[40] The distance between close-packed ligands in the smectic layers can be estimated to be 0.5−0.8 nm from the cross section of hexagonally packed alkyl chains arranged either in a row or in a triangle. Even in the most extended trans planar zigzag conformation the distance between two consecutive pyridine units in the P2VP chain must not exceed 0.25 nm.[41] Hence, for a 1:1 complex there is barely enough room in a layered structure for all ligands even in the case these are oriented up and down occupying two layers as depicted in Scheme 2a. The steric constraint can be released if the ligands get arranged around the backbone in a columnar structure. This has been observed in our previous work on the corresponding complexes.[27]

For the extreme of a low degree of neutralization, the model of Scheme 2b explains the structure observed for $P2VP_{180}$-*b*-PEO_{560} $(1\text{-H})_{0.25}$ sample rather well. The dominant feature is close packing of the ligands in single sublayers separated by an interlayer of P2VP chains. In this model several P2VP chains can be added to the polar interlayer. The ligands will prefer the upper interface and both PEO and P2VP the polar SiO_2 substrate. This asymmetry is intrinsic to Scheme 2b and explains naturally for 25% complexing a bottom layer at the substrate close to *d*/2. As complexation of the sulfonic acid with the rather basic

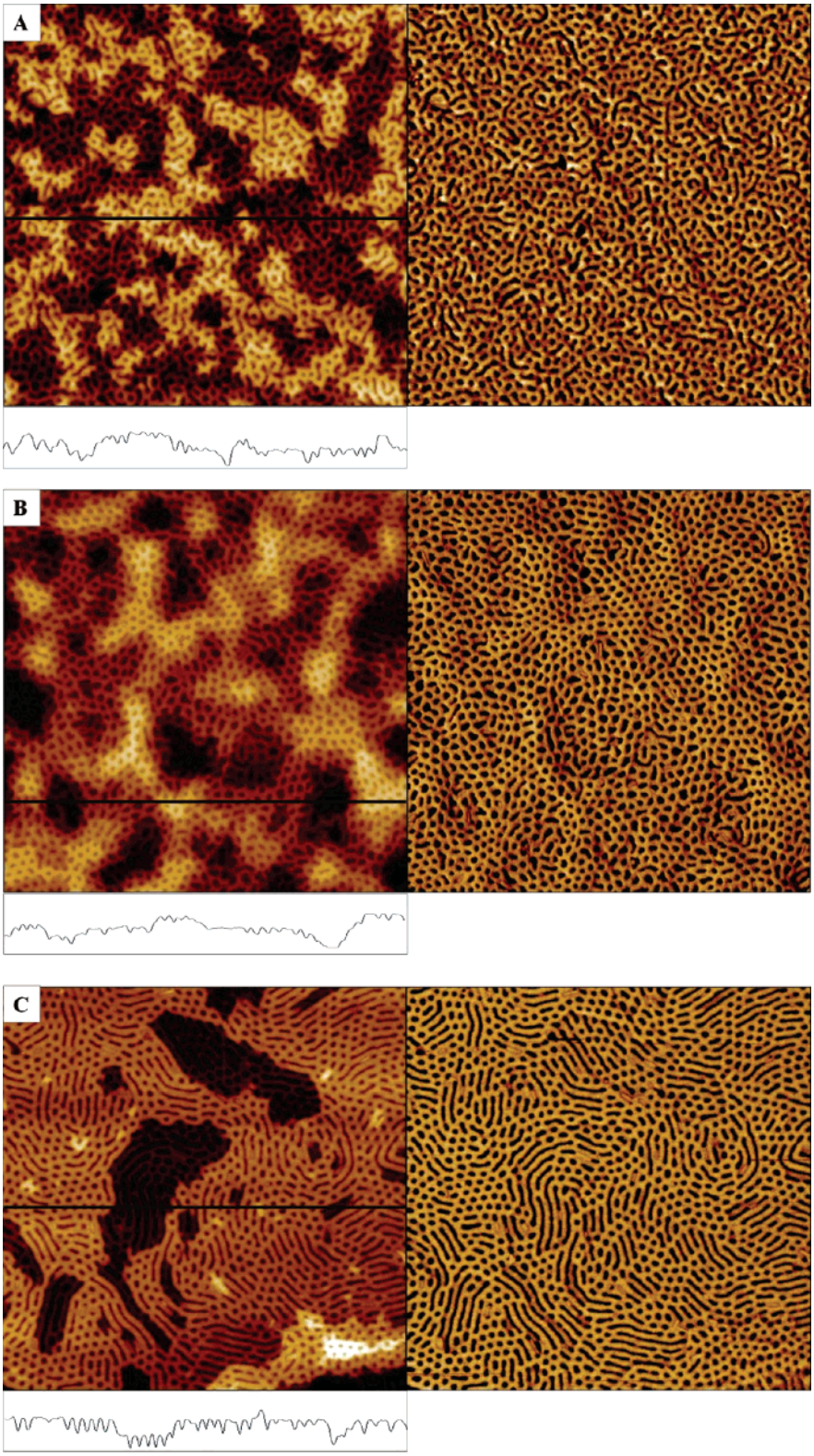

Figure 6. SFM images of $P2VP_{180}$-*b*-PEO_{560}/$(1\text{-H})_{0.25}$ complex (A) as prepared and (B) after 12 h benzene vapor annealing, (C) after 3 days benzene vapor treatment. Height image is displayed on the left and phase image on the right of each picture. *Z* range is 15 nm for (A), 40 nm for (B), and 20 nm for (C) height images. Phase scale is 25° for all images. Scan size is $2 \times 2\ \mu m^2$.

pyridine units is favored, the PEO blocks segregate in distinct cylindrical domains. A schematic model of this situation is given in Scheme 3a.

Scheme 2b corresponds to the situation we described recently for complexes of 4′-[3″,4″,5″-tris(dodecyloxy)benzoyloxy]-azobenzene-4-sulfonate and **1-H** with P4VP homopolymer. Here the P4VP chains form an interlayer between the aligned sulfonic acid molecules with a volume fraction controlled by the stochiometry.[27] In this model we may consider the interlayer as a third microphase. De Jeu et al. have described smectic−amorphous diblock copolymers as a triblock system A(BC), in which A represents the amorphous block and BC a "nanophase-

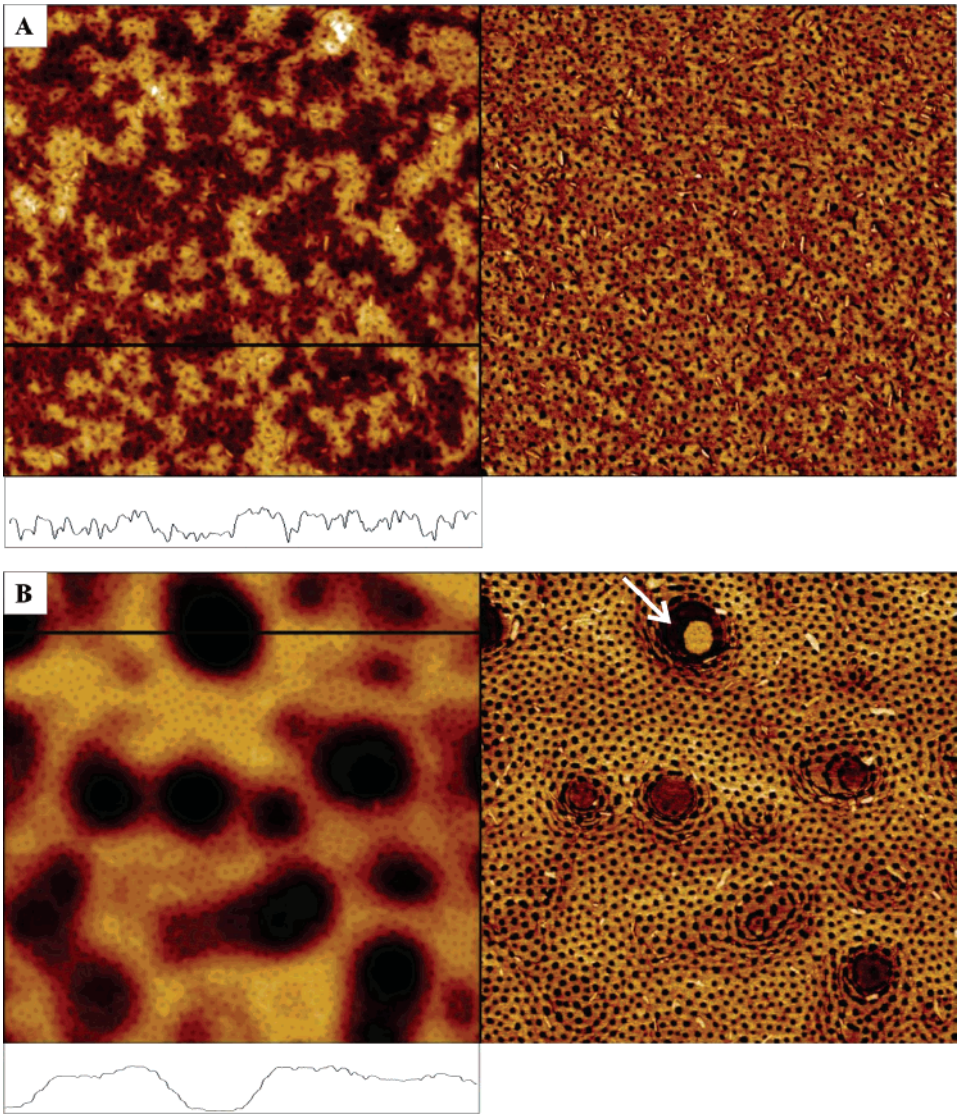

Figure 7. SFM images of $P2VP_{180}$-*b*-PEO_{560}/$(1\text{-}H)_{0.5}$ complex (A) as prepared and (B) after 12 h of benzene vapor annealing. Height image is displayed on the left and phase image on the right. *Z* range is 15 nm for (A) and 40 nm for (B). Phase scale is 30° for both images. Scan size is $2 \times 2\ \mu m^2$.

Table 3. Morphology Characteristics for 25 and 50% Complexing from SFM

degree of complexing (%)	cylinder−cylinder (centers, nm)	cylinder diameter (nm)
25	46 ± 3	28 ± 2
50	48 ± 4	22 ± 2

separated" smectic block.[18] In the present case this translates into a polar PEO block A and a BC block consisting of a polar P2VP backbone (B) sandwiched by the nonpolar ligands (C). Hence, the main separation is between C and A/B, the polymers A and B being rather compatible.

Upon increasing the degree of complexing to 50%, the cylinder-to-cylinder distance remains about the same (see Table 3), though the number of ligands increases with a factor 2. At the same time the cylinder diameter decreases (still for the same amount of PEO). Furthermore, the substrate layer increases from about *d*/2 to 0.66*d*. Obviously the steric requirements at 50% protonation along with smectic ordering suggest a transition from Scheme 2b used for 25% complexing to Scheme 2a for 50%. In that case in principle twice more ligands can be packed at the same PEO cylinder-to-cylinder distance because of the doubling along the layer normal. In addition, this doubling leads to a reduction of the number of PEO chains per smectic period with a factor 2 and thus to a reduction of the lateral PEO density with a factor $\sqrt{2} = 1.4$. The experimental ratio of cylinder diameters D25%/D50% as determined from SFM is $28/22 \approx 1.3$.

Next we come to the difference in the substrate layer between 25% and 50% complexing (see Table 2). The adsorption strength of the pyridine on silicone oxide is quite large $2-5\ k_BT$.[42] A single P2VP chain on silicone oxide is known to adopt two-dimensional conformations while its profile approaching the monomer size 0.5 nm. In the case of 25% protonation, there are still two pyridine units per pyridinium free to interact with the substrate and a *d*/2 layer at the substrate appears a reasonable assumption. When the protonation degree attains 50%, steric hindrance does not allow formation of a half layer, and the adlayer on the substrate must adopt a structure different to those in the layers above. This is confirmed by the observation of autophobic dewetting only observed for 50% protonation. It may be speculated that the 30% increase of the thickness of the bottom layer corresponds to formation of parallel half columns in this layer.

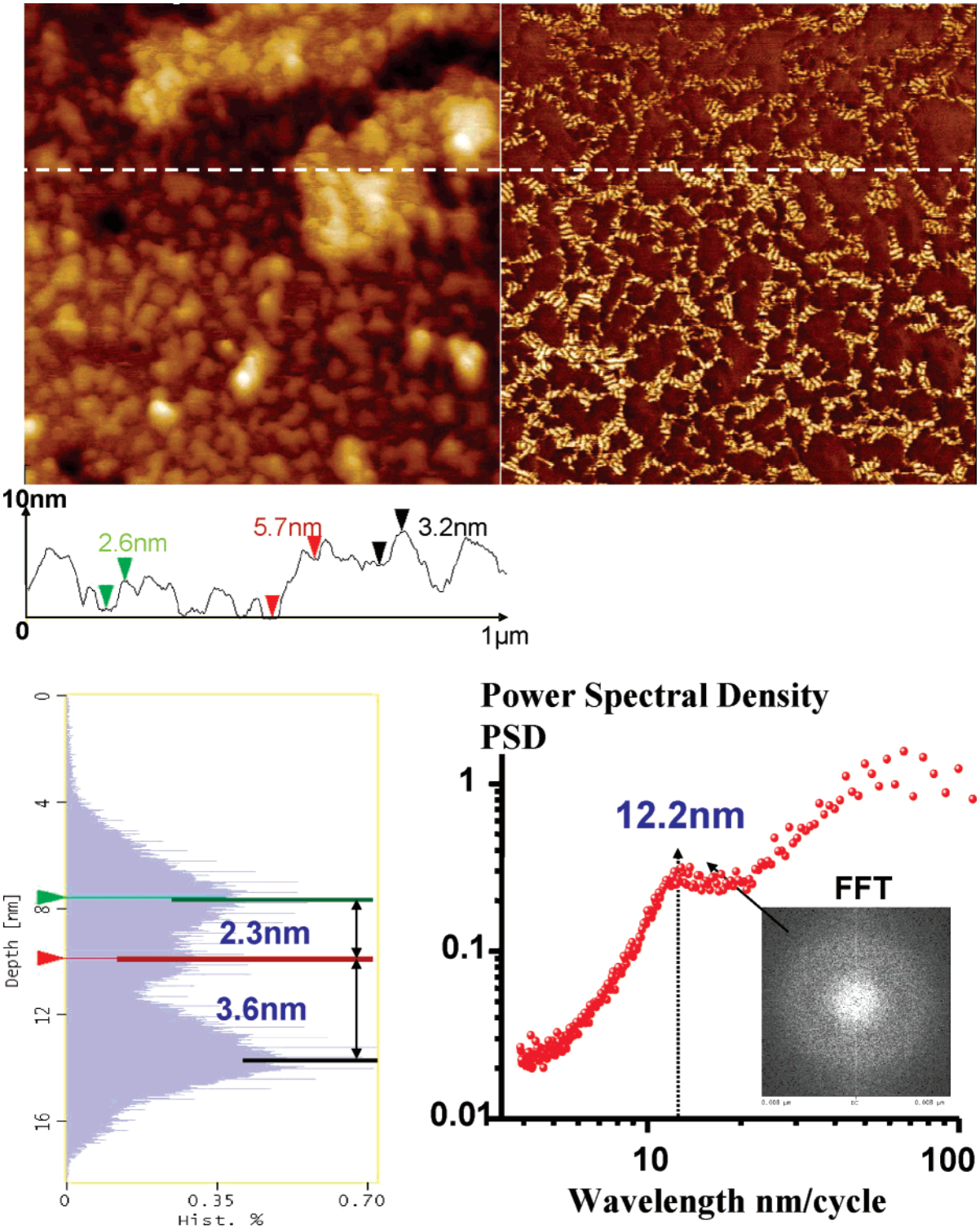

Figure 8. (a, top) SFM images of a freshly prepared film of $P2VP_{180}$-*b*-PEO_{560}/$(1\text{-H})_1$. The topography (left) indicates distinct height levels separated by ~2.3−5.9 nm (see histogram in (b)). The phase image (right) shows the islands in a "sea" of a laterally structured surface layer (alternating bright and dark stripes in the contrast). Scan size is 1 × 1 μm^2. The *Z* range is 25 nm and the full phase scale 50°. (b, bottom) Left: histogram of the height distributions from analysis of the surface topography image. Right: power spectral density as calculated from the phase image displaying a peak around 12.2 nm in accordance with the broad halo in the fast Fourier transform (inset).

Finally we discuss films of $P2VP_{180}$-*b*-PEO_{560}/$(1\text{-H})_1$. As mentioned above, steric constraints make it rather unlikely that a structure corresponding to Scheme 2 a can be adopted, and we have observed formation of a columnar structure, with the P4VP surrounded by a tube formed by the wedge-shaped sulfonic molecules for the complexes of **1-H** with P4VP. Yet, the X-ray reflectivity data demonstrate that the layer periodicity hardly varies with the degree of neutralization and excludes such a structural change for full neutralization. Furthermore, the structure observed by SFM at the air interface is peculiar (Figure 8a) as the full surface layer below the terraces is substructured with a period that exceeds the step height. Apparently, this lateral organization does not compromise layering of the film as the averaged density along the film normal (as given by XR, Figure

Scheme 2. Schematic Representation of Two Possibilities to Order the Mesogens: (a) Each Pyridine Unit Is Neutralized and the "Side Chains" Are Arranged Symmetrically with Respect to the Backbone; (b) Only a Fraction of the Pyridine Units Are Neutralized in a Statistical Manner and the P2VP Can Be Considered To Segregate in an Interphase[a]

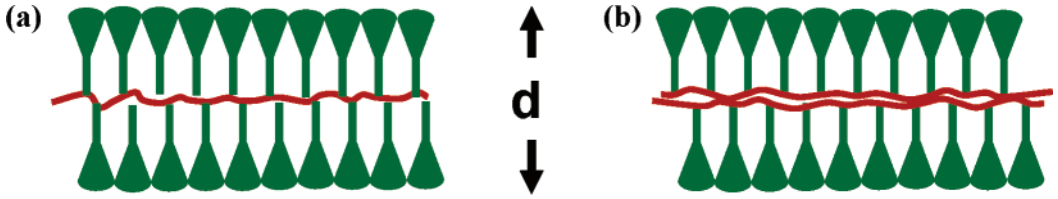

[a] Only stoichiometric protonation of the P2VP chain as in Scheme 2a leads to dissolution of the interphase.

Scheme 3. Models Proposed for the Thin Film Morphology: (a) 25% Complexing with a Smectic Layer Period of Twice *d*/2; (b) 50% Complexing with a Period *d*[a]

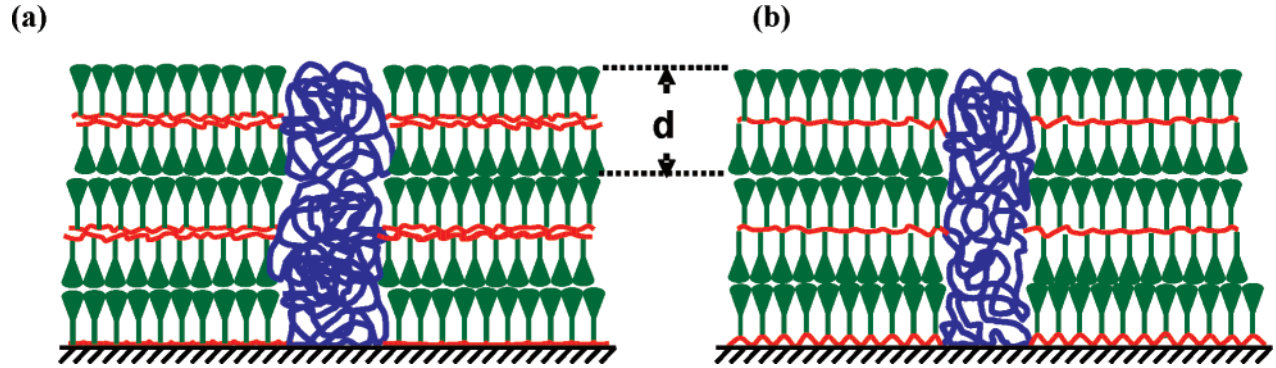

[a] Note the interphase for the 25% and the structure of the bottom layer.

3) is not affected. XR indicates also a substrate layer with a thickness of 2.4 nm, now appreciably less than half the period.[27]

Though the structural details of the block copolymer morphology for 100% complexing are not fully understood, an interesting parallel can be drawn with work on a LC−BC by Anthamatten et al.[43] They showed for a similarly high volume fraction of the LC blocks that the amorphous PS blocks segregated in bulk as small disklike domains ("compressed micelles") arranged hexagonally between the smectic layers or dispersed phase. This can be understood as the ultimate consequence of the formation of continuous smectic layers as the dominant driving force for the morphology. A similar structure could apply to our situation though only locally, as we did not observe the attendant hexagonal X-ray peaks. Regarding the substrate layer, we suggest that the thickness of it is determined by an improved ordering of the ligands. Once all the pyridine units are protonated, the polymer backbone is not bound tightly, allowing tilting of the ligand relative to the surface normal that will reduce the steric constraint on the chain and satisfy smectic ordering in the bulk of the film. This might explain thinning of the bottom layer to 0.4*d*. Certainly the precise organization of the molecules in the substrate region remains to be clarified.

Conclusions

Analysis by XR and SFM makes clear that in all present BC complexes LC ordering is preserved. In particular, the thin film structure for 25 and 50% complexing indicates for all degrees of neutralization orthogonal orientation of the wedge-shaped ligands in the proximity of the solid surface as well as at the air/polymer interface. This is in agreement with other thin film studies of smectic/amorphous BC's.[18,19]

Evidently the formation of liquid crystalline layers parallel to the interfaces is the major driving force determining the final morphology. It is remarkable that, independently of composition, the PEO microdomains of the $P2VP_{180}$-*b*-$PEO_{560}(1\text{-}H)_x$samples with $x = 0.25$ and 0.5 adopt a vertical orientation with respect to the surface and thus parallel to the LC field of the mesogens. In combination with the orthogonality of the layers and block interfaces smectic layering provides a valuable way to stabilize vertical cylinders.

Acknowledgment. This work was supported within the Maries Curie Research and Training Network "Biopolysurf" of the EU (contract CT-2004-005516). T.M. acknowledges support by the EU. K.A acknowledges support within the Graduiertenkollege 1035 Biointerface by the Deutsche Forschungsgemeinschaft.

References and Notes

(1) (a) Leibler, L. *Macromolecules* **1980**, *13*, 1602. (b) Bates, F. S.; Fredrickson, G. H. *Annu. Rev. Phys. Chem.* ***1990***, *41*, 525.
(2) Hamley, I. W. *The Physics of Block Copolymers*; Oxford: New York, 1998.
(3) Hamley, I. W. *Nanotechnology* **2003**, *14*, R39.
(4) Kellogg, G. J.; Walton, D. G.; Mayes, A. M.; Lambooy, P.; Russell, T. P.; Gallagher, P. D.; Satija, S. K. *Phys. Rev. Lett.* **1996**, *76*, 2503.
(5) Rockford, L.; Liu, Y.; Mansky, P.; Russell, T. P.; Yoon, M.; Mochrie, S. G. J. *Phys. Rev. Lett.* **1999**, *82*, 2602.
(6) Morkved, T. L.; Lu, M.; Urbas, A. M.; Ehrichs, E. E.; Jaeger, H. M.; Mansky, P.; Russell, T. P. *Science* **1996**, *273*, 931.
(7) Thurn-Albrecht, T.; Schotter, J.; Kästle, G. A.; Emley, N.; Shibauchi, T.; Krusin-Elbaum, L.; Guarini, K.; Black, C. T.; Tuominem, M. T.; Russell, T. P. *Science* **2000**, *290*, 2126.
(8) Mansky, P.; Russell, T. P.; Hawker, C. J.; Pitsikalis, M.; Mays, J. *Macromolecules* **1997**, *30*, 6810.
(9) Huang, E.; Russell, T. P.; Harrison, C.; Chaikin, P. M.; Register, R. A.; Hawker, C. J.; Mays, J. *Macromolecules* **1998**, *31*, 7641.
(10) Mansky, P.; Liu, Y.; Huang, E.; Russell, T. P.; Hawker, C. *Science* **1997**, *275*, 1458.
(11) Fasolka, M. J; Banerjee, P.; Mayes, A. M.; Pickett, G.; Balazs, A. C. *Macromolecules* **2000**, *33*, 5702.
(12) Knoll, A.; Magerle, R.; Krausch, G. *J. Chem. Phys.* **2004**, *120*, 1105.
(13) Kim, G.; Libera, M. *Macromolecules* **1998**, *31*, 2670.

(14) Kim, H.-C.; Russell, T. P. *J. Polym. Sci., Part B: Polym. Phys.* **2001**, *39*, 663.
(15) Kim, S. H.; Misner, M. J.; Xu, T.; Kimura, M.; Russell, T. P. *Adv. Mater.* **2004**, *16*, 226.
(16) Muthukumar, M.; Ober, C. K.; Thomas, E. L. *Science* **1997**, *277*, 1225.
(17) Osuji, C. O.; Chen, J. T.; Mao, G.; Ober, C. K.; Thomas, E. L. *Polymer* **2000**, *41*, 8897.
(18) de Jeu, W. H.; Séréro, Y.; Al-Hussein, M. *Adv. Polym. Sci.* **2006**, *200*, 71.
(19) Al-Hussein, M.; Séréro, Y.; Konovalov, O.; Mourran, A.; Möller, M.; de Jeu, W. H. *Macromolecules* **2005**, *38*, 9610.
(20) Wong, G. C. L.; Commandeur, J.; Fischer, H.; de Jeu, W. H. *Phys. Rev. Lett.* **1996**, *77*, 5221.
(21) Ansari, I. A.; Castelletto, V.; Mykhaylyk, T.; Hamley, I. W.; Lu, Z. B.; Itoh, T.; Imrie, C. T. *Macromolecules* **2003**, *36*, 8898.
(22) Hamley, I. W.; Castelletto, V.; Lu, Z. B.; Imrie, C. T.; Itoh, T.; Al-Hussein, M. *Macromolecules* **2004**, *37*, 4798.
(23) Figueiredo, P.; Geppert, S.; Brandsch, R.; Bar, G.; Thomann, R.; Spontak, R. J.; Gronski, W.; Samlenski, R.; Müller-Buschbaum, P. *Macromolecules* **2001**, *34*, 171.
(24) Ruokolainen, J.; Mäkinen, R.; Torkkeli, M.; Mäkelä, T.; Serimaa, R.; ten Brinke, G.; Ikkala, O. *Science* **1998**, *280*, 557.
(25) (a) Tokarev, I.; Sydorenko, A.; Minko, S.; Stamm, M. *Polym. Mater.: Sci. Eng.* **2003**, *89*, 115. (b) Sidorenko, A.; Tokarev, I.; Minko, S.; Stamm, M. *J. Am. Chem. Soc.* **2003**, *125*, 12211. (c) Tokarev, I.; Krenek, R.; Burkov, Y.; Schmeisser, D.; Sidorenko, A.; Minko, S.; Stamm, M. *Macromolecules* **2005**, *38*, 507.
(26) Zhu, X.; Tartsch, B.; Beginn, U.; Möller, M. *Chem.—Eur. J.* **2004**, *10*, 3871.
(27) Zhu, X.; Beginn, U.; Möller, M.; Gearba, R. I.; Anokhin, D. V.; Ivanov, D. I. *J. Am. Chem. Soc.* **2006**, *128*, 16928.
(28) Gohy, J.-F.; Varshney, S. K.; Antoun, S.; Jérôme, R. *Macromolecules* **2000**, *33*, 9298.
(29) (a) Magonov, S. N.; Elings, V.; Whangbo, M.-H. *Surf. Sci. Lett.* **1997**, *375*, L385. (b) Magonov, S. N.; Cleveland, J.; Elings, V.; Denley, D.; Whangbo, M.-H. *Surf. Sci.* **1997**, *389*, 201. (c) Magonov, S. N.; Reneker, D. H. *Annu. Rev. Mater. Sci.* **1997**, *27*, 175. (d) Magonov, S. N. In *Encyclopedia of Analytical Chemistry*; Meyers, R. A., Ed.; Wiley: Chichester, 2000; p 7432.
(30) Lee, J. Y.; Painter, P. C.; Coleman, M. M. *Macromolecules* **1988**, *21*, 954.
(31) Ikkala, O.; Ruokolainen, J.; ten Brinke, G.; Torkkeli, M.; Serimaa, R. *Macromolecules* **1995**, *28*, 7088.
(32) Nandan, B.; Lee, C.-H.; Chen, H.-L.; Chen, W.-C. *Macromolecules* **2005**, *38*, 10117.
(33) (a) Spatz, J. P.; Möller, M.; Noeske, M.; Behm, R. J.; Pietralla, M. *Macromolecules* **1997**, *30*, 3874. (b) Shibata, M.; Kimura, Y.; Yaginuma, D. *Polymer* **2004**, *45*, 7571.
(34) (a) Fukunaga, K.; Elbs, H.; Magerle, R.; Krausch, G. *Macromolecules* **2000**, *33*, 947. (b) Knoll, A.; Horvat, A.; Lyakhova, K. S.; Krausch, G.; Sevink, G. J. A.; Zvelindovsky, A. V.; Magerle, R. *Phys. Rev. Lett.* **2002**, *89*, 035501. (c) Elbs, H.; Drummer, C.; Abetz, V.; Krausch, G. *Macromolecules* **2002**, *35*, 5570. (d) Kim, S. H.; Misner, M. J.; Xu, T.; Kimura, M.; Russell, T. P. *Adv. Mater.* **2004**, *16*, 226. (e) Kim, S. H.; Misner, M. J.; Russell, T. P. *Adv. Mater.* **2004**, *16*, 2119.
(35) Lee, L.-T.; Woo, E. M.; Hou, S. S.; Förster, S. *Polymer* **2006**, *47*, 8350.
(36) (a) Reiter, G.; Castelein, G.; Hoerner, P.; Riess, G.; Blumen. A.; Sommer, J.-U. *Phys. Rev. Lett.* **1999**, *83*, 3844. (b) Li, L.; Séréro, Y.; Koch, M. H. J.; de Jeu, W. H. *Macromolecules* **2003**, *36*, 529.
(37) Reiter, G. *J. Polym. Sci., Part B: Polym. Phys.* **2003**, *41*, 1869.
(38) (a) Reiter, G.; Sommer, J.-S. *J. Chem. Phys.* **2000**, *112*, 4376. (b) Massa, M. V.; Carvalho, J. L.; Dalnoki-Veress, K. *Phys. Rev. Lett.* **2006**, *97*, 247802.
(39) (a) Sheiko, S.; Lermann, E.; Möller, M. *Langmuir* **1996**, *12*, 4015. (b) Sheiko, S. S.; Slangen, P.-J.; Krupers, M.; Mourran, A.; Möller, M. In *Fluorinated Surfaces, Coatings and Films*; Castner, D. G., Graigner, D. W., Eds.; ACS Symposium Series Vol 787; American Chemical Society: Washington, DC, 2001; p 71.
(40) Arnett, E. M.; Ahsan, T.; Amarnath, K. *J. Am. Chem. Soc.* **1991**, *113*, 6858.
(41) Puterman, M.; Kolpak, F. J.; Blackwell, J.; Lando, J. B. *J. Polym. Sci.: Polym. Phys. Ed.* **1977**, *15*, 805.
(42) Bemis, J. E.; Akhremitchev, B. B.; Walker, G. C. *Langmuir* **1999**, *15*, 2799.
(43) Anthamatten, M.; Wu, J.-S.; Hammond, P. T. *Macromolecules* **2001**, *34*, 8574.

MA071317N